

# Quiescent Radio Emission from Southern Late-type M and L Dwarfs and a Spectacular Radio Flare from the M8 Dwarf DENIS 1048–3956

Adam J. Burgasser<sup>1</sup>

*Department of Astrophysics, American Museum of Natural History, Central Park West at 79th Street, New York, NY 10024*

adam@amnh.org

and

Mary E. Putman

*Department of Astronomy, University of Michigan, Ann Arbor, MI 48109-1090*

mputman@umich.edu

## ABSTRACT

We report the results of a radio monitoring program conducted at the Australia Telescope Compact Array to search for quiescent and flaring emission from seven nearby Southern late-type M and L dwarfs. Two late-type M dwarfs, the M7 V LHS 3003 and the M8 V DENIS 1048–3956, were detected in quiescent emission at 4.80 GHz. The observed emission is consistent with optically thin gyrosynchrotron emission from mildly relativistic ( $\sim 1$ – $10$  keV) electrons with source densities  $n_e \lesssim 10^9 \text{ cm}^{-3}$  in  $B \gtrsim 10$  G magnetic fields. DENIS 1048–3956 was also detected in two spectacular, short-lived flares, one at 4.80 GHz (peak  $f_\nu = 6.0 \pm 0.8$  mJy) and one at 8.64 GHz (peak  $f_\nu = 29.6 \pm 1.0$  mJy) approximately 10 minutes later. The high brightness temperature ( $T_B \gtrsim 10^{13}$  K), short emission period ( $\sim 4$ – $5$  minutes), high circular polarization ( $\sim 100\%$ ), and apparently narrow spectral bandwidth of these events imply a coherent emission process in a region of high electron density ( $n_e \sim 10^{11}$ – $10^{12} \text{ cm}^{-3}$ ) and magnetic field strength ( $B \sim 1$  kG). If the two flare events are related, the apparent frequency drift in the emission suggests that the emitting source either moved into regions of higher electron or magnetic flux density; or was compressed, e.g., by twisting field lines or gas motions. This emission may be related to a recent optical flare from this source that exhibited indications of chromospheric mass motion. The quiescent fluxes from the radio-emitting M dwarfs are too bright to support the Güdel-Benz empirical radio/X-ray relations, confirming a trend previously noted by Berger et al. The violation of these relations is symptomatic of a divergence in magnetic emission trends at and beyond spectral type

---

<sup>1</sup>Spitzer Fellow

M7/M8, where relative X-ray and H $\alpha$  emission drops precipitously while relative radio emission appears to remain constant or possibly increases. With an apparent decline in chromospheric/coronal heating, the origin of hot coronal plasmas around ultracool dwarfs remains uncertain, although external sources, such as accretion from a residual disk or tidally distorted companions, remain possibilities worth exploring.

*Subject headings:* stars: activity — stars: flare — stars: low-mass, brown dwarfs — stars: individual (DENIS J104814.7-395606, LHS 102B, LHS 3003) — techniques: interferometric — radio continuum: stars

## 1. Introduction

Magnetic fields are fundamental to stars, playing an important role in early accretion, angular momentum evolution, and a number of interaction mechanisms. The presence and strength of magnetic fields above the surface of a cool star, when not directly measured from Zeeman line broadening (e.g., Saar & Linsky 1985, Johns-Krull & Valenti 1996), are generally inferred from the presence of high temperature coronal and chromospheric emission from radio to X-ray wavelengths. This high-temperature emission, which may be characterized as quiescent (stable or slowly varying) or flaring (rapid variation, high energy), must arise from nonradiative heating processes, for which magnetic activity is regarded as the most probable source. Magnetic activity is common amongst M-type stars, with the frequency and strength of quiescent H $\alpha$  emission, indicating the presence of a hot chromosphere, peaking around spectral type M7/M8 (Gizis et al. 2000; West et al. 2004). For even cooler stars and brown dwarfs, including ultracool late-type M, L, and T dwarfs (Kirkpatrick et al. 1999; Burgasser et al. 2002b), H $\alpha$  emission declines rapidly, both in strength and frequency, so that few field objects later than type L5 exhibit any optical emission whatsoever (Gizis et al. 2000; Burgasser et al. 2002a). Similar trends are also found in quiescent X-ray emission (Neuhäuser et al. 1999; Fleming, Giampapa & Garza 2003).

The reduction of chromospheric and coronal emission in ultracool dwarfs is broadly consistent with theoretical expectations. The cool, dense atmospheres of these objects imply low ionization fractions and thus high electric resistivities, so that magnetic field lines are largely decoupled from the upper atmosphere (Meyer & Meyer-Hofmeister 1999; Mohanty et al. 2002; Gelino et al. 2002). As a result, the generation and propagation of magnetic stresses, which can lead to magnetic reconnection followed by electron/ion acceleration, is inhibited at the stellar surface. The generation of the magnetic field itself may also be impeded, as the fully convective interiors of objects with masses  $M \lesssim 0.3 M_{\odot}$  (Chabrier & Baraffe 1997) inhibits the standard  $\alpha\Omega$  dynamo mechanism, although other dynamo mechanisms — turbulent (Durney, De Young, & Roxburgh 1993) or  $\alpha^2$  dynamos (Rädler et al. 1990) — may be sufficient.

The occurrence of flaring emission does not appear to drop off as rapidly as quiescent emission, as objects as late as spectral type L5 (Hall 2002a,b; Gizis 2002; Liebert et al. 2003,  $T_{eff} \approx 1700$

K), and possibly T6 (Burgasser et al. 2000, 2002a,  $T_{eff} \approx 1000$  K), have been detected in outburst. Optical flares, both line and continuum emission, typically last on order hours and have duty cycles (percentage of time in strong emission) of  $\lesssim 1\text{--}7\%$  (Reid et al. 1999; Gizis et al. 2000; Liebert et al. 2003). These flares have been detected on objects with no observable quiescent emission (Basri & Marcy 1995; Reid et al. 1999). X-ray flares have been detected in field objects down to spectral types M9/M9.5 (Fleming, Giampapa & Schmitt 2000; Rutledge et al. 2000; Schmitt & Liefke 2002; Hambaryan et al. 2004). The presence of flaring, high-energy emission from very late-type dwarfs is strong evidence that magnetic fields are present. However, based on the theoretical expectations outlined above, it still remains unclear how magnetic flaring energy is transmitted through largely neutral atmospheres (Mohanty et al. 2002).

Given these activity trends near the M/L dwarf boundary, nonthermal magnetic radio emission from cool dwarf stars and brown dwarfs has largely been assumed to be exceedingly weak. This expectation is supported by the Güdel-Benz relations (Güdel & Benz 1993; Benz & Güdel 1994, hereafter GB relations), an empirical correlation between radio and X-ray luminosities that holds over several orders of magnitude over much of the low-mass stellar main sequence and for interacting binary/active systems. The GB relations predict radio fluxes  $f_\nu \lesssim 1 \mu\text{Jy}$  for nearby ultracool M dwarfs (Berger 2002, hereafter B02), undetectable with current instrumentation. Early radio studies of the latest-type dwarfs appeared to confirm this prediction (e.g., Krishnamurthi, Leto & Linsky 1999). However, Berger et al. (2001, hereafter B01) detected both quiescent and flaring radio emission from the 500 Myr M9 brown dwarf LP 944-20, an object that is both very cool ( $T_{eff} \approx 2150$  K; Dahn et al. 2002) and undetected in quiescent X-rays (Rutledge et al. 2000). This radio emission violates the GB relations by roughly four orders of magnitude. Three other late-type dwarfs spanning M8.5 to L3.5 were subsequently detected in quiescent and flaring radio emission (B02), at levels much higher than expected from the GB relations. These observations indicate that both magnetic fields and sustained coronal plasmas are present above the photospheres of ultracool dwarfs at and below the Hydrogen burning limit, and point to a fundamental change in the magnetic emission process at low  $T_{eff}$ .

To further explore nonthermal emission from ultracool dwarfs, we have used the Australia Telescope Compact Array (ATCA) to search for radio emission from seven nearby, late-type M and L dwarfs in the Southern hemisphere. In § 2 we describe the sample, observations, and data reduction procedures. Detection of quiescent emission from two late-type M dwarfs are discussed and analyzed in § 3. One of the quiescent sources, the M8 dwarf DENIS 1048–3956, was also detected in two short, powerful flares in both of the frequency bands observed; this emission is discussed in § 4. In § 5 we examine possible trends of radio emission with spectral type, rotation, and the existence of optical quiescent and/or flaring emission; and speculate on the origin of coronal plasma above cool photospheres. Results are summarized in § 6.

## 2. Observations

### 2.1. The Sample

Seven nearby ultracool dwarfs in the Southern hemisphere were selected for observation; their properties are summarized in Table 1. The primary selection criteria were (1) spectral type M7 or later, where the GB relations appear to break down (B02); and (2) proximity to the Sun. As such, our sample spans the spectral type range M7 to L5 and have distance measurements or spectrophotometric estimates of 11 pc or closer (with the exception of 2MASS 1139–3159, see below). Detailed descriptions of the targets are as follows:

*LHS 102B*: Identified by Goldman et al. (1999), this object is a common proper motion companion to the M3.5 V high-proper motion star LHS 102 (a.k.a. GJ 1001), which has a parallactic distance measurement of  $9.55 \pm 0.10$  pc (van Altena, Lee, & Hoffleit 1995). Its L5 spectral type suggests that it is cool enough to be substellar ( $T_{eff} \approx 1800$  K; Leggett et al. 2002), although the absence of Li I absorption at 6708 Å implies  $M > 0.06 M_{\odot}$  (Rebolo, Martín, & Magazzu 1992). Goldman et al. (1999) estimate  $M = 0.072 M_{\odot}$  for an age of 5 Gyr; i.e., at the Hydrogen burning limit. High-resolution spectroscopy by Basri et al. (2000) shows that LHS 102B is a rapid rotator, with  $v \sin i = 32.5 \pm 2.5$  km s<sup>-1</sup>. Weak H $\alpha$  emission is also seen in its optical spectrum. Golimowski et al. (2004) have recently resolved this source as a 0".086 (0.8 AU), equal-mass binary.

*SSSPM 0109–5100*: Identified by Lodieu, Scholz, & McCaughrean (2002) in the SuperCOSMOS Sky Survey (Hambly et al. 2001), this object has a near-infrared spectrum consistent with an L2 dwarf. Scholz & Meusinger (2002) estimate a distance of  $\sim 13$  pc based on its photographic *R* and *I* magnitudes and spectral type. Using the  $M_J$ /spectral type relation of Cruz et al. (2003) and 2MASS photometry (Cutri et al. 2003), we estimate a distance of  $\sim 10$  pc. With no published optical spectrum available, it is unknown as to whether this source has quiescent H $\alpha$  emission or Li I absorption.

*2MASS 0835–0819*: Identified and optically classified by Cruz et al. (2003), this L5 dwarf has an estimated  $T_{eff} \sim 1700$  K, based on the temperature/spectral type relation of Golimowski et al. (2004). Like LHS 102B, 2MASS 0835–0819 is likely at or below the substellar limit. Li I absorption is not seen in its low-resolution optical spectrum, however, nor is quiescent H $\alpha$  emission. Cruz et al. (2003) estimate the distance of 2MASS 0835–0819 at  $\sim 8$  pc.

*DENIS 1048–3956*: Identified in the DENIS survey (Epchtein et al. 1997) by Delfosse et al. (2001), this bright source ( $J = 9.54 \pm 0.04$ ) has a high proper motion,  $\mu = 1''.529 \pm 0''.017$  yr<sup>-1</sup>. Neuhäuser et al. (2002) measure a parallactic distance of  $4.6 \pm 0.3$  pc (see also Deacon & Hambly 2001), making this the closest star in our sample. Originally classified M9 by Delfosse et al. (2001), we adopt the revised classification of M8 from Gizis (2002). High resolution optical spectroscopy by Fuhrmeister & Schmitt (2004) indicate  $v \sin i = 25 \pm 2$  km s<sup>-1</sup>, consistent with measurements by Delfosse et al. (2001), making DENIS 1048–3956 another rapid rotator. Quiescent and variable H $\alpha$  emission has been detected from this object (Delfosse et al. 2001; Neuhäuser et al. 2002; Gizis 2002),

while Fuhrmeister & Schmitt (2004) have detected a massive optical flare, including blueshifted components indicative of mass motion. Schmitt & Liefke (2004) report an X-ray luminosity upper limit of  $L_X < 2 \times 10^{26}$  erg s<sup>-1</sup> based on the absence of this source in the Röntgen Satellite (ROSAT) all-sky survey catalog.

*2MASS 1139–3159*: Identified by Gizis (2002), this M8 dwarf is the only object in our sample with a spectrophotometric distance beyond 11 pc. 2MASS 1139–3159 was chosen for its possible membership in the  $\sim 10$  Myr TW Hydra Association (de la Reza et al. 1989; Kastner et al. 1997), which would make it a young, very low-mass ( $M \sim 0.025 M_\odot$ ) brown dwarf. Optical spectroscopy from Gizis (2002) shows both H $\alpha$  and He I (6679 Å) emission, along with low surface gravity features indicative of a young, low-mass brown dwarf. Li I absorption has not been reported, however.

*LHS 3003*: With a parallactic distance of  $6.56 \pm 0.15$  pc (Ianna 1995), this M7 dwarf is a nearby and well-studied system. LHS 3003 was originally identified as a cool star by Ruiz et al. (1990), who observed a full sequence of Balmer H I emission while this object was in a flare state. Quiescent H $\alpha$  emission has also been observed at the level  $\log(L_{H\alpha}/L_{bol}) \approx -4.3$  (Tinney & Reid 1998; Mohanty & Basri 2003). In addition, ROSAT observations by Schmitt, Fleming, & Giampapa (1995) detected this object in soft X-rays (0.1–2.4 keV) at the level of  $L_X \approx 2 \times 10^{26}$  erg s<sup>-1</sup>, or  $\log(L_X/L_{bol}) \approx -4.0$ . High resolution optical spectroscopy by Mohanty & Basri (2003) indicate that this source is a slow rotator, with  $v \sin i = 8.0 \pm 2.5$  km s<sup>-1</sup>.

*2MASS 1534–1418*: Identified by Gizis (2002), this M8 dwarf has a spectrophotometric distance of  $\sim 11$  pc. Quiescent H $\alpha$  emission is seen in its low-resolution optical spectrum, but there has been no additional follow-up of this source published in the literature.

## 2.2. Data Acquisition and Reduction

All observations were conducted with ATCA in its fully extended 6A configuration (baselines of 0.63–5.94 km) during two runs on 2002 May 16–17 and 2002 Nov 29–Dec 2 (UT). A log of observations is given in Table 2. Sources were tracked in continuum mode simultaneously at 4.80 and 8.64 GHz (6 and 3 cm) using the broadest bandwidth available (128 MHz over 32 channels, binned to 13 independent channels) and sampling every 10 s. Nearby secondary calibrators selected from the ATCA Calibrator Catalog<sup>1</sup> were interspersed every 30–45 minutes for relative flux and phase correction, and the primary calibrators PKS B0823–500 and PKS B1934–638 were observed for absolute calibration at the beginning and/or end of each target cycle. Sources were tracked for 10–12 hr depending on the declination, with on-source times of roughly 8–10 hr each.

Visibility data were reduced in the MIRIAD environment<sup>2</sup> using standard routines. First,

---

<sup>1</sup>See <http://www.narrabri.atnf.csiro.au/calibrators/c007/atcat.html>.

<sup>2</sup>See <http://www.atnf.csiro.au/computing/software/miriad/index.html>.

poor baselines in the target and calibrator sources were flagged by visual inspection, both before and after phase and flux calibration, by checking antenna leakage ( $\lesssim 1\%$ ), phase and flux stability of primary and secondary calibrators, and secondary calibrator polarization ( $\lesssim 3\%$ ). Phase and flux calibration of the target observations were tied to the secondary calibrators, which were in turn tied to the primary calibrators. The fully calibrated visibility datasets were then inverted and cleaned using the MIRIAD routines *INVERT*, *CLEAN*, and *RESTORE* to produce imaging data for source verification and measurement. Radio fluxes were measured using the *IMFIT* routine, while uncertainties were estimated from the standard deviation of the imaging data over a  $\sim 2' \times 2'$  area without sources near the target position. For DENIS 1048–3956, these uncertainties are slightly higher than expected due to sidelobes from the bright radio source NVSS 104748–395053 (Condon et al. 1998;  $f_{1.4\text{GHz}} = 120 \pm 4$  mJy),  $7.2'$  northwest of the target. Because of its complex double-lobed morphology, we were unable to model and subtract this background source from the visibility data. However, its influence in the region of DENIS 1048–3956 is minimal (Figure 2), and the source was not present in the 8.64 GHz band nor in the Stokes Q, U, or V polarization images.

For time series data (§ 4), visibilities for each polarization (Stokes I, Q, U, and V) were independently averaged across all baselines to measure the total radio flux, and monochromatic flux densities were computed by averaging the central nine channels ( $\Delta\nu = 72$  MHz) in the frequency domain. Uncertainties in the time series data were estimated from the standard deviation of the averaged visibilities over 30 min intervals (in the absence of flaring emission); i.e., assuming slow variation in the total source and background radio emission in each field. These uncertainties were typically of order 1 mJy per 10 s time bin.

### 3. Quiescent Emission

#### 3.1. Detections

For our targeted observations, we adopted a somewhat less stringent  $3\sigma$  limit (0.10–0.12 mJy) for source detection than the typical 4–5 $\sigma$  limits used for survey work (e.g., Richards et al. 1998). Only two of our targets had spatially coincident quiescent radio sources above this threshold in the 4.80 GHz band, LHS 3003 and DENIS 1048–3956. Imaging data for these two sources in the Stokes I polarization at both frequencies are shown in Figures 1 and 2. Note that the images for DENIS 1048–3956 do not include visibility data during the periods of flaring observed from this object (§ 4). The radio flux peaks detected near these sources are found to be within the mean beam size of the predicted positions of the targets as determined from 2MASS astrometry (accurate to within  $0''.3$ ; Cutri et al. 2003) and proper motion measurements from the literature (Tinney 1996; Neuhäuser et al. 2002). The relatively bright source ( $f_\nu = 0.27 \pm 0.04$  mJy) coincident with LHS 3003 has a faint  $\sim 5''$  extension toward the northeast which also appears in the 8.64 GHz image. We cannot rule out noise as the origin of this extended emission. The fainter source ( $f_\nu = 0.14 \pm 0.04$  mJy)

coincident with DENIS 1048–3956 has a shape consistent with the beam profile. No significant, spatially coincident radio sources were found at 8.64 GHz for any of the targets. All measurements are given in Table 3.

At the faint flux levels probed by our observations, background confusion is an important consideration. We therefore estimated the probability that the detected 4.80 GHz sources are associated with LHS 3003 and DENIS 1048–3956 by computing the expected number of background sources ( $N$ ) with similar brightnesses present within the ATCA beam. A 6 cm Very Large Array (VLA) survey of the Lockman Hole by Ciliegi et al. (2003) identified 28 sources (corrected for completeness to 28.6 sources) with  $f_\nu > 0.113$  mJy in a  $0.087 \text{ deg}^2$  area, implying an integrated source density  $N \approx 2.5 \times 10^{-5} \text{ arcsec}^{-2}$  for  $0.1 \lesssim f_\nu \lesssim 20$  mJy. This is consistent with results from other deep 6 cm surveys (Altshuler 1986; Donnelly, Partridge, & Windhorst 1987; Fomalont et al. 1991). Based on the beam sizes listed in Table 2, this background density implies a confusion probability  $1 - e^{-N} \lesssim 0.3\%$  and  $0.2\%$  for LHS 3003 and DENIS 1048–3956, respectively, ruling out confusion with high confidence. We therefore conclude that quiescent emission from LHS 3003 and DENIS 1048–3956 at 4.80 GHz was detected.

Examination of the Stokes Q, U and V 4.80 GHz images for LHS 3003 and DENIS 1048–3956 show no significant sources. However, these non-detections give only weak constraints on the polarization of the quiescent emission. Circular polarization upper limits ( $3\sigma$ ) at 4.80 GHz are  $\Pi_V \equiv V/I < 44\%$  and  $< 86\%$  for LHS 3003 and DENIS 1048–3956, respectively.

### 3.2. Characterizing the Quiescent Emission

The flux densities of the two detected M dwarfs imply frequency-dependent radio luminosities  $L_{\nu,q} \equiv 4\pi f_\nu d^2 \approx (4 - 13) \times 10^{12} \text{ erg s}^{-1} \text{ Hz}^{-1}$  (Table 3), where  $d$  is the distance to the source. These values are similar to measurements for hotter M stars as well as many of the late-type dwarfs detected by B02, although most of those detections were made at 8.46 GHz. The non-detections in our sample generally have luminosity upper limits brighter than the detections.

The brightness temperature of the radio emission at frequency  $\nu$ ,

$$T_B = 2 \times 10^9 (f_\nu/\text{mJy})(\nu/\text{GHz})^{-2} (d/\text{pc})^2 (\mathcal{L}/R_{Jup})^{-2} \text{ K}, \quad (1)$$

(Dulk 1985) provides a measure of the energetics of the emitting electron population.  $\mathcal{L}$  is the length scale of the emitting region, normalized here to the typical radii of very low mass stars and brown dwarfs,  $R_* \sim 0.1 R_\odot \sim 1 R_{Jup} \approx 7 \times 10^9 \text{ cm}$  (Burrows et al. 2001). Assuming M-type stellar coronal dimensions,  $\mathcal{L} \sim (2 - 3) \times R_*$  (Benz, Aref, & Güdel 1995), the detected radio emissions imply  $T_B \approx (3 - 30) \times 10^7 \text{ K}$  (Table 3). The temperature of the emitting electrons,  $T_e$ , is related to the brightness temperature by  $T_e = T_B$  for optically thick emission, and  $T_e = \tau_\nu T_B$  for optically thin emission, where  $\tau_\nu$  is the frequency-dependent optical depth of emission. The absence of emission at 8.64 GHz for any of these sources implies that the quiescent flux peaks near or below 4.80 GHz,

so that  $T_e \lesssim T_B \sim 10^7\text{-}10^8$  K. These values are similar to coronal (ion) plasma temperatures of other late-type M dwarfs derived from X-ray measurements (Giampapa et al. 1996; Rutledge et al. 2000; Feigelson et al. 2002; Fleming, Giampapa & Garza 2003). Note that a more extended corona, such as that proposed by Fleming, Giampapa & Garza (2003) for the M8 dwarf VB 10 ( $\mathcal{L} \lesssim 20R_*$ ) would imply brightness temperatures that are significantly lower. On the other hand, VLBI measurements of the M-type flare stars EQ Peg B and AD Leo find  $\mathcal{L} \lesssim 2R_*$  (Benz, Alef, & Güdel 1995; Leto et al. 2000). For lack of further observational constraints, we assume the source scale used above.

The inferred brightness temperatures imply a population of mildly relativistic (1-10 keV) electrons in the emitting region. Hence, gyrosynchrotron emission is likely the source of the observed quiescent flux, a mechanism commonly prescribed for persistent emission from late-type stars (Güdel 2002). We can estimate the total radio luminosity of each source by assuming emission below a peak frequency,  $\nu_{pk}$ , scales as  $\nu^{2.5}$ , and emission above  $\nu_{pk}$  scales as  $\nu^\alpha$ , where  $\alpha = 1.22 - 0.9\delta$  for a power-law electron distribution  $n(E) \propto E^{-\delta}$  (Dulk & Marsh 1982; Dulk 1985). Typical coronal values of  $\delta \approx 2 - 4$  (Güdel 2002) imply  $\alpha \approx -1.5$ , consistent with our 8.64 GHz upper limits ( $\alpha < -0.4$  and  $-1.2$ ). Assuming  $\nu_{pk} \approx 5$  GHz and emission over a harmonic range of 100 ( $\nu_{pk}/10 < \nu < 10\nu_{pk}$ ), we estimate  $L_R = \int L_{\nu,q} d\nu \approx (3 - 10) \times 10^{22}$  ergs s $^{-1}$ , or  $\log L_R/L_{bol} \approx -7.3$  and  $-7.7$  for LHS 3003 and DENIS 1048–3956, respectively. These values are similar to those obtained by B02 for their late-type M dwarf quiescent detections.

For gyrosynchrotron emission, the peak frequency of the radio flux for a power-law electron distribution is related to the electron density ( $n_e$ ), length scale and magnetic field strength ( $B$ ) of the emitting region as<sup>3</sup>

$$\nu_{pk} \approx 16.6 n_e^{0.23} \mathcal{L}^{0.23} B^{0.77} \text{ kHz} \quad (2)$$

(Dulk 1985), where we have assumed  $\delta \sim 3$  and an average pitch angle  $\theta = \pi/3$  (Güdel 2002). Using the length scale above and again assuming  $\nu_{pk} \approx 5$  GHz, Eqn. 2 reduces to  $B \approx 11 n_9^{-0.3}$ , where  $n_9 = n_e / (10^9 \text{ cm}^{-3})$ . We can further use the requirement that Razin-Tsytovich suppression (Tsytovich 1951; Razin 1960) is minimal at the frequencies observed, implying that emission occurs above a minimum frequency  $\nu_{min}$ , and hence

$$\nu_{pk} \gtrsim \nu_{min} \gtrsim \frac{\nu_p^2}{\nu_c} \approx 29 \frac{n_9}{B} \text{ GHz} \quad (3)$$

for mildly relativistic electrons (Dulk 1985). Here,  $\nu_p \equiv (n_e e^2 / \pi m_e)^{1/2} \approx 0.28 \sqrt{n_9}$  GHz is the fundamental plasma frequency and  $\nu_c = eB / 2\pi m_e c \approx 2.8B$  MHz is the cyclotron frequency. Combining Eqns. 2 and 3 yields  $n_e \lesssim 2 \times 10^9 \text{ cm}^{-3}$  and  $B \gtrsim 10$  G for both LHS 3003 and DENIS 1048–3956.

---

<sup>3</sup>Note that the relations for gyrosynchrotron emission given in Dulk (1985) and Güdel (2002) assume a lower electron energy cutoff of 10 keV, whereas we estimate energies down to 1 keV for our sources. Derivation of accurate expressions in the lower energy regime are beyond the scope of this paper, and we assume our estimates to be accurate at the order-of-magnitude level.



The quiescent magnetic field estimates, likely accurate only to within an order of magnitude, are roughly in agreement with those of B02 for their ultracool dwarf detections. Our electron density estimates, on the other hand, are  $\sim 10^3$  times smaller. *Chandra* and XMM-Newton grating observations of the M3.5 V AD Leo yield coronal electron density upper limits more consistent with our estimates,  $n_e \lesssim 10^{10} - 10^{11} \text{ cm}^{-3}$  (van den Besselaar et al. 2003), although the structure of the coronal region of this star may be quite different than that of our cooler sources.

## 4. Flaring Emission from DENIS 1048–3956

### 4.1. Detection and Characterization of the Flares

Time series analysis of all targets was performed to search for variability and flare events. Only one source was detected above our  $\sim 3$  mJy sensitivity threshold ( $3\sigma$  standard deviation in 30 s binned visibilities), the quiescent emitter DENIS 1048–3956. As shown in Figure 3, this object underwent two strong and rapid flares, one each at 4.80 and 8.64 GHz. Flaring emission is particularly strong at 8.64 GHz, and can be seen in the visibility data. These flares were very short-lived, with durations of  $\tau \sim 4 - 5$  minutes in each band; and occurred roughly 10 minutes apart, peaking at 14:15:15 and 14:25:16 (UT) for the 4.80 and 8.64 GHz emission, respectively. There was no significant emission in the opposite frequency for either of the flares, indicating narrow-band emission. Peak flux densities,  $f_{\nu,f}$ , estimated from Gaussian fits to the unbinned time series data, were  $6.0 \pm 0.8$  mJy and  $29.6 \pm 1.0$  mJy at 4.80 and 8.64 GHz, respectively. These fluxes are over ten times brighter than the radio flares observed on LP 944-20 by B01, which lies at a similar distance as DENIS 1048–3956. Finally, both flares were highly circularly polarized. Figure 4 compares the Stokes Q, U, and V polarizations for both flares. Neither were detected in the Stokes Q and U polarizations. Peak Stokes Q and U fluxes at 4.80 GHz have  $1\sigma$  upper limits of 1.1 and 1.2 mJy, respectively, implying peak polarizations  $\Pi_Q \equiv Q/I < 18\%$  and  $\Pi_U \equiv U/I < 20\%$ . At 8.64 GHz,  $\Pi_Q$  and  $\Pi_U$  are both  $< 3\%$  ( $1\sigma$ ). On the other hand, Stokes V polarizations in both bands were essentially unity at the peak of the flares (c.f., Figures 3 and 4). Hence, essentially all of the emission is concentrated in circular polarization.

Given the unique nature of these flares, we carefully checked that emission originated from the source by examining the visibility images over the entire observation period. Distinct fringes, expected from an unresolved point source observed with parallel baselines, are seen with maximum intensity at the position of DENIS 1048–3956 in imaging data that includes the flare period, and the fringes are spaced and oriented in accordance with the alignment of the ATCA at the time of the flare emission. The flares do not arise from the bright radio source NVSS 104748–395053, as no flare emission is found at the position of this source in the imaging data. Indeed, the fringes are most obvious in the Stokes V images in which there is no interfering emission from NVSS 104748–395053. We therefore conclude that the flaring radio emission originates from DENIS 1048–3956 itself.

## 4.2. Coherent Emission

The strong, rapid, narrow-band, and highly polarized flares detected from DENIS 1048–3956 are quite different than those observed from late-type M and L dwarfs by B02, which had longer flare periods ( $\sim 6$ –25 min) and somewhat less polarized ( $\sim 30$ –66%) emission. Flares detected on LP 944-20 by B01 exhibited coincident peaks at 4.86 and 8.46 GHz, as opposed to the temporally offset flares seen here. Furthermore, the brightness temperatures of the DENIS 1048–3956 flares are very high,  $T_B = (1.1 \pm 0.2) \times 10^{10} (\mathcal{L}/R_*)^{-2}$  and  $(1.7 \pm 0.2) \times 10^{10} (\mathcal{L}/R_*)^{-2}$  K for the 4.80 and 8.64 GHz flares, respectively. Peak brightness temperatures for other radio flaring late-type M and L dwarfs are a factor of 10 or more less. On the other hand, the DENIS 1048–3956 flaring emission is quite similar to rapid ( $\lesssim 10$  min), highly polarized ( $\gtrsim 60\%$ ) flares seen on earlier-type active M stars, including the M5.5 V UV Cet A (Benz, Conway, & Güdel 1998; Bingham, Cairns, & Kellett 2001), the M4 V DO Cep (White, Jackson, & Kundu 1989), and AD Leo (Stepanov et al. 2001). The last source exhibited a rapid ( $\sim 1$  min) burst at 4.85 GHz with a peak flux  $f_{\nu,f} \approx 300$  mJy,  $T_B \sim 5 \times 10^{10} (\mathcal{L}/R_*)^{-2}$  K, and nearly 100% circular polarization, similar in scale and energetics to the emission seen on DENIS 1048–3956. Stepanov et al. (2001) argue that the high temperature and polarization of this flare is the result of a coherent emission process, as has been argued for other rapid, high energy and high polarization flares (Bingham, Cairns, & Kellett 2001). The properties of the DENIS 1048–3956 flares indicate coherent emission as well.

Two mechanisms are generally considered for coherent processes in cool stellar coronae: electron cyclotron maser (ECM) and plasma emission. Both produce narrow bandwidth, highly polarized, and highly energized radio bursts. The propagation of this emission is problematic at the frequencies observed here, however, as free-free and gyroresonance absorption from ambient (thermal) electrons will suppress emergent radiation (Dulk 1985). Indeed, coherent emission above 5 GHz is exceedingly rare (Güdel 2002). However, radiation can escape from regions with sufficiently high density gradients. The optical depth for free-free absorption is

$$\tau_{ff} \approx 15 T^{-3/2} (\nu/\text{GHz})^2 \mathcal{L}_n \quad (4)$$

(Dulk 1985), where  $\mathcal{L}_n \equiv n_e/\nabla n_e$  is the density gradient scale in cm. For DENIS 1048–3956, assuming that the ambient electron temperature is that derived from the quiescent emission,  $\tau_{ff}$  is less than unity for  $\mathcal{L}_n \lesssim 3 \times 10^8$  cm  $\sim 0.04 R_*$ , implying  $T_B \gtrsim 10^{13}$  K for  $\mathcal{L} \sim \mathcal{L}_n$ . These values are similar to those derived for the AD Leo flare, and again suggests similar emission mechanisms.

Stepanov et al. (2001) argue that plasma emission is more likely in the case of AD Leo given the higher degree of gyroresonance absorption occurring for ECM emission. Plasma emission is peaked at the plasma frequency, implying  $n_e \approx 3 \times 10^{11}$  and  $9 \times 10^{11}$  cm $^{-3}$  for the 4.80 and 8.64 GHz flares of DENIS 1048–3956, respectively. Razin-Tsytoich suppression implies  $B \lesssim 2 - 3$  kG. On the other hand, if ECM is responsible (as is argued for bursts on UV Cet; Bingham, Cairns, & Kellett 2001), emission at  $\nu_c$  implies  $B = 1.7 - 3.1$  kG and  $n_e \lesssim 10^{11}$  cm $^{-3}$  (constraining  $\nu_p/\nu_c \lesssim 0.5$ ; Dulk 1985). Hence, we estimate  $B \sim 1$  kG and  $n_e \sim 10^{11}$ – $10^{12}$  cm $^{-3}$  in the flaring region, similar to values derived for the AD Leo flare (Stepanov et al. 2001) but much larger than estimates from

the quiescent emission of this source. The amplification of the magnetic field in the flaring region could arise from twisted loops associated with magnetic reconnection sites. The higher electron densities are consistent with Solar flaring loop plasmas, which are 10–100 times more dense than quiescent regions (Canfield et al. 1990).

### 4.3. A Single Flare Event with Frequency Drift?

The unique nature, temporal proximity, and non-simultaneous emission during the DENIS 1048–3956 flares strongly suggests that they are related. We propose that the two flares are in fact snapshots of a single narrow bandwidth flaring event whose source region evolved in such a way as to cause a frequency drift in the emission. Such narrow-band frequency drift has been previously observed in radio dynamic spectra of active stars (Jackson et al. 1987; Bastian 1990). Assuming simplistically that the propagation is linear in time, the temporal spacing of the emission implies a drift rate  $\dot{\nu} \approx +6.4 \text{ MHz s}^{-1}$ , of the same order as drift rates observed from a 10 minute radio flare observed from the active M6 star UV Cet (Jackson et al. 1987). The similar (possible) drift rates and timescales suggest that the emission from both stars could arise from analogous processes.

Assuming for the purposes of discussion that a frequency drift is present, the shift toward higher emission frequencies indicates that the source region evolved toward conditions of higher magnetic field strength and/or electron density. This transition could arise from physical movement of the source — e.g., infalling into regions of higher density and/or field strength — or a modification of the source environment — e.g., compaction of the emitting region or a compression of field lines. In either case, a frequency drift implies  $\dot{n}_e \approx +10^9 \text{ cm}^{-3} \text{ s}^{-1}$  for plasma emission. We can assign a drift or compaction velocity ( $v_s$ ) to the emitting region by assuming  $\mathcal{L}_n \approx n_e v_s / n_e \lesssim 0.04 R_*$ , so that  $v_s \lesssim 5 \text{ km s}^{-1}$ . This value is similar to the velocity of redshifted components seen in line emission from a massive optical flare from DENIS 1048–3956 (Fuhrmeister & Schmitt 2004). While the long chain of assumptions used here cannot prove a connection between the optical and radio flaring, the suggested agreement in the kinematics is intriguing. It is also possible that the radio flux is emerging from optically thick emission to optically thin emission, consistent with the  $\nu^{2.7}$  dependence between the 4.80 and 8.64 GHz peak fluxes. This emergence of the source region may be the result of a clearing away of overlying absorbing plasma, possibly related to the highly blueshifted ( $v \sim 100 \text{ km s}^{-1}$ ) components of the optical flare detected by Fuhrmeister & Schmitt (2004).

The peak luminosities,  $L_{\nu,f}$  from the flaring emission are  $1.5 \times 10^{14}$  and  $7.5 \times 10^{14} \text{ erg s}^{-1} \text{ Hz}^{-1}$  for the 4.80 and 8.64 GHz spikes, respectively. The total radio luminosity depends on the frequency response of the emission. At one extreme, if we assume that the two flare events are independent and confined to the observed frequency bands ( $\Delta\nu = 72 \text{ MHz}$ ), then  $L_R \approx L_{\nu,f} \Delta\nu = 6 \times 10^{22} \text{ erg s}^{-1}$ , roughly equivalent to the persistent component. On the other hand, if the flare emission is the result of a drifting source, the emission band could be as broad as  $\Delta\nu \approx \dot{\nu} \tau \approx 2 \text{ GHz}$ . Assuming a Gaussian frequency distribution with a full width at half maximum of 2 GHz, the equivalent radio

luminosity is ten times greater, approaching  $10^{-6}L_{bol}$ . Similarly, the total energy released in the flaring emission may range from  $10^{24}$  erg (observed emission) to  $> 10^{26}$  erg for a drifting source.

## 5. Discussion

### 5.1. Radio Emission Trends

The detection of quiescent emission from a handful of ultracool M and L dwarfs is surprising in itself, but perhaps more interesting is that this emission may in fact be common. B02 found that the relative quiescent radio luminosity of their detected late-type sources,  $L_R/L_{bol}$ , was constant or increasing with spectral type out to type L3.5. This trend is contrary to the observed  $H\alpha$  emission, which weakens rapidly beyond spectral type M7/M8 (Gizis et al. 2000; West et al. 2004); and quiescent X-ray emission, which appears to turn over around the same spectral types (Fleming, Giampapa & Garza 2003). Figure 5 compares the ratios  $L_{\nu,q}/L_{bol}$  and  $L_{H\alpha}/L_{bol}$  versus spectral type for field stars with spectral types M2 to L6. Values for  $L_{\nu,q}$  at 3 or 6 cm were obtained from the literature (Linsky & Gary 1983; White, Jackson, & Kundu 1989; Güdel & Benz 1993; Krishnamurthi, Leto, & Linksy 1999; Leto et al. 2000, B01; B02) and our own observations. Bolometric luminosities as a function of spectral type were derived from a seventh order polynomial fit to empirical values for M and L dwarfs in the 8 pc sample (Reid & Hawley 2000) and from Golimowski et al. (2004). Values for  $L_{H\alpha}/L_{bol}$  are from Hawley, Gizis, & Reid (1996); Gizis et al. (2000), and Burgasser et al. (2002a). The trend of increasing relative radio luminosity is clearly apparent in this data, extending well beyond the drop in  $H\alpha$  emission. A linear fit to radio detections with spectral types M3 to M9 yields

$$\log L_{\nu,q}/L_{bol} = -18.1 + 0.11 \times \text{SpT}, \quad (5)$$

where  $\text{SpT}(M3) = 3$ ,  $\text{SpT}(M9) = 9$ , etc. This is similar to the relation diagrammed in Figure 6b of B02. Furthermore, the single L dwarf radio detection (the L3.5 dwarf 2MASS 0036+1821) is consistent with an extrapolation of this trend. One caveat, however, is that many of the radio quiescent detections are close to the sensitivity limits of the observations. Hence, non-detection upper limits are not strong constraints for lower levels of emission (or non-emission), which may be orders of magnitude below this line. Nonetheless, with fourteen radio-emitting late-type M and L dwarfs within 12 pc of the Sun having detections or upper limits within 0.5 dex of this line, there are strong indications of a general trend.

The few sources that have radio emission upper limits below this line were closely examined by B02, who found that a dominant fraction were slowly rotating ( $v \sin i < 10 \text{ km s}^{-1}$ ), late-type M dwarfs. This, argued B02, suggests a correlation between rotation and radio emission analogous to the well-known activity-rotation relation for F-K main sequence stars (Pallavicini et al. 1981; Noyes et al. 1984). Again, our observations lend some support to this conclusion, as DENIS 1048–3956 is clearly a rapid rotator with  $v \sin i = 25 \pm 2 \text{ km s}^{-1}$ . However, the brighter radio detection in

our sample, LHS 3003, has  $v \sin i = 8.0 \pm 2.5 \text{ km s}^{-1}$  (Mohanty & Basri 2003), equivalent to the similarly-typed M7 dwarf VB 8 which has an upper limit on its radio flux well below Eqn. 5 ( $\log L_{\nu,q}/L_{bol} < -18.4$ ; Krishnamurthi, Leto, & Linsky 1999). Of course, as  $v \sin i$  provides only a lower limit on the actual rotation velocity, it is possible that LHS 3003 is a rapid rotator viewed close to pole-on. However, the L5 2MASS 1507–1627, which was undetected by B02 to a 3 cm limit of  $\log L_{\nu,q}/L_{bol} < -16.8$  (compared to  $-16.5$  from Eqn. 6), is a rapid rotator, with  $v \sin i = 27 \pm 6 \text{ km s}^{-1}$  (Bailer-Jones 2004). Hence, rotation may not be the only factor driving radio emission.

Turning to the presence of  $H\alpha$  emission, it is interesting to note that both of our detected sources are quiescent  $H\alpha$  emitters and therefore have appreciable chromospheres. On the other hand, both 2MASS 1139–3159 and 2MASS 1534–1418, which were not detected in the radio, also exhibit quiescent  $H\alpha$  emission; while two of the four sources detected by B02 (BRI 0021–0214 and 2MASS 0036+1821) have little or no quiescent  $H\alpha$  flux. There is therefore no clear correlation of radio coronal emission with optical chromospheric emission. On the other hand, two of the four late-type M and L dwarfs detected by B02 and both sources detected in our study have been observed in strong  $H\alpha$  or X-ray flaring emission. This includes the rapidly-rotating M9.5 dwarf BRI 0021–0214 which exhibits no quiescent  $H\alpha$  emission (Basri & Marcy 1995; Reid et al. 1999). Since flaring emission is fairly rare, it is possible that the other radio detections are flare stars that have not yet been observed in optical or X-ray emission. It is again important to consider contrary examples, however. These include the actively flaring stars LHS 2243 (Gizis et al. 2000, M8) and LHS 2065 (Martín & Ardila 2001; Schmitt & Liefke 2002, M9), which have 3 cm luminosity limits  $\log L_{\nu,q}/L_{bol} < -17.0$  and  $-17.5$ , respectively (Krishnamurthi, Leto, & Linsky 1999, B02). Compared to predicted values from Eqn. 5,  $-17.2$  and  $-17.1$ , these upper limits are below, but still fall within 0.5 dex of, this possible radio emission/spectral type trend. Interestingly, both of these undetected flare stars are slowly rotating, with  $v \sin i < 12 \text{ km s}^{-1}$  (Mohanty & Basri 2003). Future monitoring observations of radio detected and undetected sources will be needed to explore any correlation between quiescent radio emission and optical flaring.

## 5.2. Violations of the Güdel-Benz Relations

As discussed in § 1, one of the interesting revelations of the quiescent and flaring radio emission from LP 944-20 and other late-type M and L dwarfs was the gross violation of the radio/X-ray GB relations. The sources detected in our sample also violate these relations. The ROSAT X-ray detection of LHS 3003, assuming it to be quiescent emission, implies  $L_{\nu,q} \approx 10^{-15.5} L_X \approx 6 \times 10^{10} \text{ erg s}^{-1} \text{ Hz}^{-1}$ , about 200 times fainter than measured here. Upper limits on the X-ray emission from DENIS 1048–3956 predict radio fluxes  $\sim 60$  times fainter than our detection. These deviations are not as extreme as those reported by B02 for the M9 dwarfs LP 944-20 and BRI 0021–0214 (3-4 orders of magnitude), suggesting that the shift away from the radio/X-ray empirical trend occurs gradually around spectral type M7.

The reason for this deviation is likely related to the emission trends diagrammed in Figure 5.

If X-ray and optical emission are correlated, as suggested by the relation  $L_X \sim L_{H\alpha}$  typical for M stars (Reid, Hawley, & Mateo 1995; Fleming, Giampapa & Garza 2003), the divergence of H $\alpha$  and radio emission trends at and beyond spectral types M7 would be consistent with violations of the GB relations. The implication is that high-energy electrons in magnetic fields are present around ultracool dwarfs, but that coronal and chromospheric plasma heating is somehow suppressed or attenuated. While electron densities still appear to be relatively high in the radio-emitting coronal region (although this depends on the adopted emission mechanism), chromospheric densities might be reduced in accordance with the increasingly neutral photospheres of these objects. This would explain the divergence of H $\alpha$  and radio emission trends, but not necessarily the apparent divergence between X-ray and radio emission. The latter may require a substantial decrease in the temperature of coronal plasmas around ultracool stars and brown dwarfs, perhaps due to a reduction in the energetics of whatever nonthermal processes supply the radio-emitting region with ionized material.

## 6. Where do the Coronal Plasmas Come From?

The presence of magnetic fields around late-type M, L, and even cooler brown dwarfs is in itself not surprising, as large-scale fields are generated by the Solar giant planets despite having  $T_{eff} \lesssim 130$  K. Indeed, the dynamo mechanism for a gas giant such as Jupiter, driven by convective motions in the fluid metallic Hydrogen interior (Stevenson 2003), may be a good analogy for the dynamo mechanism employed by ultracool stars and brown dwarfs. A more intriguing mystery is the origin and retention of coronal and chromospheric plasmas in the context of increasingly neutral photospheres. Electron precipitation is the dominant loss mechanism of the coronal plasma, occurring over timescales ( $\tau_e$ ) of order minutes (Linsky & Gary 1983; Kundu et al. 1987). The presence of quiescent radio emission necessitates a constant replenishment of coronal plasma, but how is this plasma supplied? The most commonly prescribed source is microflaring: short, rapid, bursting emission that continually accelerates electrons to coronal energies and may in fact comprise the observed quiescent flux (Güdel 2002). Evidence of substantial variability or polarization in quiescent radio emission would provide support for this interpretation. While our detections are too close to the sensitivity limit to usefully test this prediction, the detection of multiple flaring events on LP 944-20 (B01) and highly variable emission from the L3.5 2MASS 0036+1821 (B02) are certainly supportive. Furthermore, the possible correlation between radio emission and optical flaring suggested above could provide a means of moving ionized material into the upper atmosphere.

External sources for coronal plasma should also be considered. One possibility is accretion from the interstellar medium (ISM), which can be expressed as

$$\left(\frac{dN_e}{dt}\right)_{in} \sim \epsilon n_{ISM} \pi \mathcal{L}^2 V, \quad (6)$$

where  $N_e \sim n_e \mathcal{L}^3$  is the total number of electrons in the corona,  $n_{ISM} \approx 0.07 \text{ cm}^{-3}$  is the density of the ISM (Paresce 1984),  $V \sim 30 \text{ km s}^{-1}$  is the relative dwarf/ISM velocity (roughly the typical space velocity of a late-type disk dwarf; Gizis et al. 2000), and  $\epsilon$  is a numerical factor encompassing

the fraction of ISM material acquired and ionized by the passing dwarf. A sustained coronal plasma requires  $dN_e/dt = -(dN_e/dt)_{precip} + (dN_e/dt)_{in} = 0$ , where  $(dN_e/dt)_{precip} \sim N_e/\tau_e$ . Even assuming<sup>4</sup>  $\epsilon = 1$ , the condition of equilibrium results in a coronal plasma density  $n_e \sim 10^{-2} \text{ cm}^{-3}$ , several orders of magnitude less than observed. Hence, ISM accretion is not a viable method.

Another possibility is ongoing accretion from a circumstellar disk. Assuming the accretion of hydrogen gas at a rate  $\dot{M}$ ,

$$\left(\frac{dN_e}{dt}\right)_{in} \sim \frac{\epsilon \dot{M}}{m_p}, \quad (7)$$

where  $m_p = 1.7 \times 10^{-24} \text{ g}$  is the proton mass. For an accretion rate of  $10^{-10} M_\odot \text{ yr}^{-1}$ , derived for 50 Myr M-type brown dwarfs in the R CrA association (Barrado y Navascués, Mohanty, & Jayawardhana 2004), an equilibrium coronal density of  $5 \times 10^{10} \text{ cm}^{-3}$  can be maintained for  $\epsilon = 0.1$ . Hence, young stars and brown dwarfs could sustain coronal plasmas through accretion alone. On the other hand, this mechanism may not be viable for older field dwarfs, as disk accretion drops off dramatically for ages  $\gtrsim 50 \text{ Myr}$  (Bouvier, Forestini, & Allain 1997).

Finally, plasma accretion could originate from a close companion undergoing steady mass loss. This mechanism is responsible for Jupiter’s auroral plasma, the majority of which is supplied from the tidally stressed moon Io. If planetary systems analogous to Jupiter’s moon system exist around very low-mass stars and brown dwarfs, accretion from those objects is a viable, albeit rare possibility (due to tidal circularization and the special geometry of the Io-Europa-Ganymede system). For Jupiter, the current flow between Io and Jupiter also gives rise to strong, variable decametric radio emission (Burke & Franklin 1955; Bigg 1964; Goldreich & Lynden-Bell 1969), and it is possible that coherent emission from DENIS 1048–3956 is a high-frequency analogue of this interaction. Searches for similar radio emission from systems with known extrasolar planets have thus far turned up negative (Winglee, Dulk, & Bastian 1986; Bastian, Dulk, & Leblanc 2000), although most of these systems contain early-type, relatively inactive primaries. If the primary is a magnetically active late-type M star, the likelihood of ECM emission at GHz frequencies may be increased. We note that magnetic star-planet interactions have been suggested as a means of inducing mass ejection (Ip, Kopp, & Hu 2004), a possible explanation for the apparent chromospheric mass motion observed in the optical flare of DENIS 1048–3956 (Fuhrmeister & Schmitt 2004).

These speculative hypotheses for the origin and retention of coronal plasmas reflect both poor observational constraints and limited modelling of the coronae of cool dwarf stars and brown dwarfs. One point is certain, however; substantial and sustained ionized material is present in the upper atmospheres of these objects despite the observed trends in optical and X-ray emission and theoretical expectations. Future studies of the variability, physical extent, and spectral characteristics of the radio emission may help ascertain the nature of this hot coronal gas.

---

<sup>4</sup>Perfect acquisition of ISM material is unlikely for a number of reasons, including the presence of stellar winds and shielding by the magnetosphere. This assumption is therefore overoptimistic.

## 7. Summary

From a sample of seven late-type M and L dwarfs within 20 pc from the Sun, we have detected two late-type M dwarfs, LHS 3003 and DENIS 1048–3956, in quiescent emission at 4.80 GHz. This emission indicates that both magnetic fields ( $B \gtrsim 10$  G) and sustained coronal plasmas ( $n_e \lesssim 10^9$  cm $^{-3}$ ) are present in these sources, contrary to theoretical expectations. Coupled with VLA detections of ultracool dwarfs by B01 and B02, there is an apparent trend for radio emission to remain constant or increasing over spectral types M5 to M9, and possibly into the L dwarf regime, coincident with a rapid decline in optical (H $\alpha$ ) and X-ray emission. The deviation in these activity trends explains gross violations of the GB relations, and indicates a shift in the magnetic emission mechanisms of active stars and brown dwarfs around spectral type M7/M8.

We also detected DENIS 1048–3956 in two strong, rapid, and highly polarized flares at both 4.80 and 8.64 GHz, each 4-5 minutes in duration separated by 10 minutes. These flares have a coherent emission origin, and their similarity to highly polarized bursts from other active M stars suggests plasma or ECM emission from a small ( $\mathcal{L} \lesssim 0.04 R_*$ ), high density ( $n_e \sim 10^{11}$ - $10^{12}$  cm $^{-3}$ ), highly magnetic ( $B \sim 1$  kG) region. The temporal proximity of the flaring events suggests a large-scale frequency drift in the emission, possibly due to motion or compression of the emitting region. Both persistent and flaring radio emissions make up a small ( $L_R \sim 10^{-7}$ - $10^{-6} L_{bol}$ ) but nontrivial fraction of the total luminosity from this low-mass star.

To date, seven nearby ultracool dwarfs spanning spectral types M7 to L5 have been reported in quiescent and flaring radio emission. All of the detected sources lie within 12 pc of the Sun, implying that a significant fraction of cool dwarfs overall are in fact radio-emitters. While the relative radio emission shows some indication of increasing with spectral type, it remains unclear as to whether there is any strict correlation with rotation or the presence of optical emission, although rapidly rotating and/or flaring sources are more often radio-emitters. Clearly, a larger sample of well-characterized objects is needed to explore these trends. While the detection of radio emission proves the presence of magnetic fields and coronal plasmas on ultracool dwarfs, there remains substantial uncertainty as to the strength, scale, stability, and origin of the fields and plasmas, which should be explored with further observations and theoretical work.

A. J. B. and M. E. P. would like to thank members of the Australia Telescope National Facility for their support and hospitality during the observations, and in particular our duty astronomers Jules Harnett and Jess O’Brien. We also thank N. McClure-Griffiths for assisting in observations during our May 2002 run. We give special thanks to our anonymous referee, whose extensive comments allowed us to greatly improve the original manuscript. A. J. B. acknowledges useful discussions with T. Ayres, E. Berger, A. Burrows, M. Giampapa, J. Liebert, J. Linsky, A. Melatos, J. Turner, & R. Webster during the preparation of this manuscript. Support for this work was provided by NASA through Hubble Fellowship grants from the Space Telescope Science Institute, which is operated by the Association of Universities for Research in Astronomy, Incorporated,



under NASA contract NAS5-26555; and through the Spitzer Fellowship Program. The Australia Telescope is funded by the Commonwealth of Australia for operation as a National Facility managed by CSIRO.

Facilities: ATCA.

## REFERENCES

- Altshuler, D. R. 1986, *A&AS*, 65, 267
- Bailer-Jones, C. A. L. 2004, *A&A*, 419, 703
- Barrado y Navascués, D., Mohanty, S., & Jayawardhana, R. 2004, *ApJ*, 604, 284
- Basri, G., & Marcy, G. W. 1995, *AJ*, 109, 762
- Basri, G., Mohanty, S., Allard, F., Hauschildt, P. H., Delfosse, X., Martín, E. L., Forveille, T., & Goldman, B. 2000, *ApJ*, 538, 363
- Bastian, T. S. 1990, *SoPh*, 130, 265
- Bastian, T. S., Dulk, G. A., & LeBlanc, Y. 2000, *ApJ*, 545, 1058
- Benz, A. O., Aef, W., & Güdel, M. 1995, *A&A*, 298, 187
- Benz, A. O., Conway, J., & Güdel, M. 1998, *A&A*, 331, 596
- Benz, A. O., & Güdel, M. 1994, *A&A*, 285, 621
- Berger, E. 2002, *ApJ*, 572, 503 (B02)
- Berger, E., et al. *Nature*, 410, 338 (B01)
- Bessell, M. S. 1991, *AJ*, 101, 662
- Bigg, E. K. 1964, *Nature*, 203, 1088
- Bingham, R., Cairns, R. A., & Kellett, B. J. 2001, *A&A*, 370, 1000
- Bouvier, J., Forestini, M., & Allain, S. 1997, *A&A*, 326, 1023
- Burgasser, A. J., Liebert, J., Kirkpatrick, J. D., & Gizis, J. E. 2002a, *AJ*, 123, 2744
- Burgasser, A. J., Kirkpatrick, J. D., Reid, I. N., Liebert, J., Gizis, J. E., & Brown, M. E. 2000, *AJ*, 120, 473
- Burgasser, A. J., et al. 2002b, *ApJ*, 564, 421

- Burke, B. F., & Franklin, K. L. 1955, *JGR*, 60, 213
- Burrows, A., Hubbard, W. B., Lunine, J. I., & Liebert, J. 2001, *Rev. of Modern Physics*, 73, 719
- Canfield, R. C., Metcalf, T. R., Zarro, D. M., & Lemen, J. R. 1990, *ApJ*, 348, 333
- Chabrier, G., & Baraffe, I. 1997, *A&A*, 327, 1039
- Ciliegi, P., Zamorani, G., Hasinger, G., Lehmann, I., Szokoly, G., & Wilson, G. 2004, *A&A*, 398, 901
- Condon, J. J., Cotton, W. D., Greisen, E. W., Yin, Q. F., Perley, R. A., Taylor, G. B., & Broderick, J. J. 1998, *AJ*, 115, 1693
- Cruz, K. L., Reid, I. N., Liebert, J., Kirkpatrick, J. D., & Lowrance, P. J. 2003, *AJ*, 126, 2421
- Cutri, R. M., et al. 2003, Explanatory Supplement to the 2MASS All Sky Data Release, <http://www.ipac.caltech.edu/2mass/releases/allsky/doc/explsup.html>
- Dahn, C. C., et al. 2002, *AJ*, 124, 1170
- Deacon, N. R., & Hambly, N. C. 2001, *A&A*, 380, 148
- de la Reza, R., Torres, C. A. O., Quast, G., Castilho, B. V., & Vieira, G. L. 1989, *ApJ*, 343, L61
- Delfosse, X., et al. 2001, *A&A*, 336, L13
- Donnelly, R. H., Partridge, R. B., & Windhorst, R. A. 1987, *ApJ*, 321, 94
- Dulk, G. A. 1985, *ARA&A*, 23, 169
- Dulk, G. A., & Marsh, K. A. 1982, *ApJ*, 259, 350
- Durney, B. R., De Young, D. S., & Roxburgh, I. W. 1993, *SoPh*, 145, 207
- Epchtein, N., et al. 1997, *The Messenger*, 87, 27
- Fiegelson, E. D., Broos, P., Gaffney, J. A., III, Garmire, G., Hillenbrand, L. A., Pravdo, S. H., Townsley, L., & Tsuboi, Y. 2002, *ApJ*, 574, 258
- Fleming, T. A., Giampapa, M. S., & Garza, D. 2003, *ApJ*, 594, 982
- Fleming, T. A., Giampapa, M. S., & Schmitt, J. H. M. M. 2000, *ApJ*, 533, 372
- Fomalont, E. B., Windhorst, R. A., Kristian, J. A., & Kellermann, K. I. 1991, *ApJ*, 475, L5
- Fuhrmeister, B., & Schmitt, J. H. M. M. 2004, *A&A*, 420, 1079
- Gelino, C. R., Marley, M. S., Holtzman, J. A., Ackerman, A. S., & Lodders, K. 2002, *ApJ*, 577, 433

- Giampapa, M. S., Rosner, R., Kashyap, V., Fleming, T. A., Schmitt, J. H. M. M., & Bookbinder, J. A. 1996, *ApJ*, 463, 707
- Gizis, J. E. 2002, *ApJ*, 575, 484
- Gizis, J. E., Monet, D. G., Reid, I. N., Kirkpatrick, J. D., Liebert, J., & Williams, R. 2000, *AJ*, 120, 1085
- Goldman, B., et al. 1999, *A&A*, 351, L5
- Goldreich, P., & Lynden-Bell, D. 1969, *ApJ*, 156, 59
- Golimowski, D. A., et al. 2004, *AJ*, 127, 3516
- Güdel, M. 2002, *ARA&A*, 40, 217
- Güdel, M., & Benz, A. O. 1993, *ApJ*, 405, L63
- Hall, P. B. 2002a, *ApJ*, 564, L89
- . 2002b, *ApJ*, 580, L77
- Hambaryan, V., Staude, A., Schwobe, A. D., Scholz, R.-D., Kimeswenger, S., & Neuhäuser, R. 2004, *A&A*, 415, 265
- Hambly, N. C., et al. 2001, *MNRAS*, 326, 1279
- Hawley, S. L., Gizis, J. E., & Reid, I. N. 1996, *AJ*, 112, 2799
- Ianna, P. A. 1995, in *The Bottom of the Main Sequence and Beyond*, ed. C. G. Tinney (Heidelberg: Springer-Verlag), p. 138
- Ip, W.-H., Kopp, A., & Hu, J.-H. 2004, *ApJ*, 602, L531
- Jackson, P. D., Kundu, M. R., & White, S. M. 1987, *ApJ*, 316, L85
- Johns-Krull, C. M., & Valenti, J. A. 1996, *ApJ*, 459, L95
- Kastner, J. H., Zuckerman, B., Weintraub, D. A., & Forveille, T. 1997, *Science*, 277, 67
- Katsova, M. M., Badalyan, O. G., & Livshits, M. A. 1987, *Astron. Zh.*, 64, 1243
- Kirkpatrick, J. D., et al. 1999, *ApJ*, 519, 802
- Krishnamurthi, A., Leto, G., & Linsky, J. L. 1999, *AJ*, 118, 1369
- Kundu, M. R., Jackson, P. D., White, S. M., & Melozzi, M. 1987, *ApJ*, 312, 822
- Lane, B. F., Boden, A. F., & Kulkarni, S. R. 2001, *ApJ*, 551, L81

- Leggett, S. K., Hauschildt, P. H., Allard, F., Geballe, T. R., & Baron, E. 2002, *MNRAS*, 332, 78
- Leto, G., Pagano, I., Linsky, J. L., Rodonóno, M., & Umana, G. 2000, *A&A*, 359, 1035
- Liebert, J., Kirkpatrick, J. D., Cruz, K. L., Reid, I. N., Burgasser, A. J., Tinney, C. G., & Gizis, J. E. 2003, *AJ*, 125, 343
- Liebert, J., Kirkpatrick, J. D., Reid, I. N., & Fisher, M. D. 1999, *ApJ*, 519, L345
- Linsky, J. L., & Gary, D. E. 1983, *ApJ*, 274, 776
- Lodieu, N., Scholz, R.-D., & McCaughrean, M. J. 2002, *A&A*, 389, L20
- Luyten, W. J. 1979a, *LHS Catalogue: A Catalogue of Stars with Proper Motions Exceeding 0<sup>o</sup>.5 Annually* (Minneapolis: Univ. Minn. Press)
- Martín, E. L., & Ardila, D. R. 2001, *AJ*, 121, 2758
- Meyer, F., & Meyer-Hofmeister, E. 1999, *A&A*, 341, L23
- Mohanty, S., & Basri, G. 2003, *ApJ*, 583, 451
- Mohanty, S., Basri, G., Shu, F., Allard, F., & Chabrier, G. 2002, *ApJ*, 572, 469
- Neuhäuser, R., et al. 1999, *A&A*, 343, 883
- Neuhäuser, R., et al. 2002, *AN*, 323, 447
- Noyes, R. W., Hartmann, L. W., Baliunas, S. L., Duncan, D. K., & Vaughan, A. H. 1984, *ApJ*, 279, 763
- Pallavicini, R., Golub, L., Rosner, R., Vaiana, G. S., Ayres, T., & Linsky, J. L. 1981, *ApJ*, 248, 279
- Paresce, F. 1984, *AJ*, 89, 1022
- Rädler, K. -H., Wiedemann, E., Bradenberg, A., Meinel, R., & Tuominen, I. 1990, *A&A*, 239, 413
- Razin, V. A. 1960, *Radiofiz.*, 3, 584
- Rebolo, R., Martín, E. L., & Magazzu, A. 1992, *ApJ*, 389, L83
- Reid, I. N., & Hawley, S. L. 2000, *New Light on Dark Stars* (Chichester: Praxis)
- Reid, I. N., Hawley, S. L., & Mateo, M. 1995, *MNRAS*, 272, 828
- Reid, I. N., Kirkpatrick, J. D., Gizis, J. E., & Liebert, J. 1999, *ApJ*, 527, L105
- Richards, E. A., Kellermann, K. I., Fomalont, E. B., Windhorst, R. A., & Partridge, R. B. 1998, *AJ*, 116, 1039

- Rutledge, R. E., Basri, G., Martín, E. L., & Bildsten, L. 2000, ApJ, 538, L141
- Ruiz, M. T., Anguita, C., Maza, J., & Roth, M. 1990, AJ, 100, 1270
- Saar, S. H., & Linsky, J. L. 1985, ApJ, 299, L47
- Schmitt, J. H. M. M., Fleming, T. A., & Giampapa, M. S. 1995, ApJ, 450, 392
- Schmitt, J. H. M. M., & Liefke, C. 2002, A&A, 382, L9
- . 2004, A&A, 417, 651
- Scholz, R.-D., & Meusinger, H. 2002, MNRAS, 336, L49
- Ségransan, D., Kervella, P., Forveille, T., & Queloz, D. 2003, A&A, 397, L5
- Stepanov, A. V., Kliem, B., Zaitsev, V. V., Fürst, E., Jessner, A., Krüger, A., Hildebrandt, J., & Schmitt, J. H. M. M. 2001, A&A, 374, 1072
- Stevenson, D. J. 2003, Earth Planet. Sci. Lett., 208, 1
- Tinney, C. G. 1996, MNRAS, 281, 644
- Tinney, C. G., & Reid, I. N. 1998, MNRAS, 301, 1031
- Tsyтович, V. N. 1951, Vestn. Mosk. Univ. Phys., 11, 27
- van Altena, W. F., Lee, J. T., & Hoffleit, E. D. 1995, The General Catalog of Trigonometric Stellar Parallaxes, 4<sup>th</sup> Edition (New Haven: Yale Univ. Obs.)
- van den Besselaar, E. J. M., Raassen, A. J. J., Mewe, R., van der Meer, R. L. J., Güdel, M., & Audard, M. 2003, A&A, 411, 587
- West, A. A., et al. 2004, AJ, 128, 426
- White, S. M., Jackson, P. D., & Kundu, M. R. 1989, ApJS, 71, 895
- Winglee, R. M., Dulk, G. A., & Bastian, T. S. 1986, ApJ, 309, L59

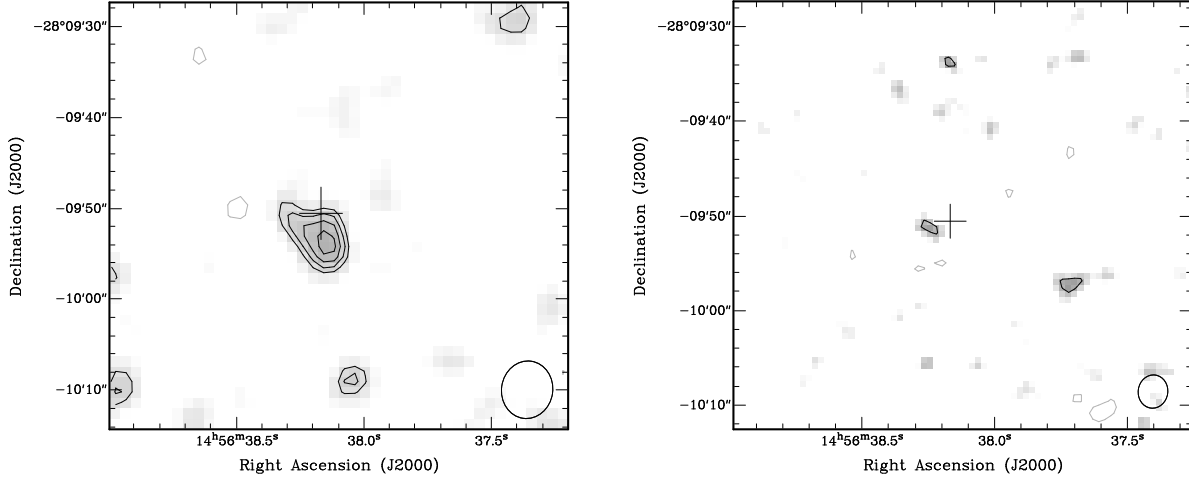


Fig. 1.— Cleaned Stokes I images of the M7 dwarf LHS 3003 at 4.80 (left) and 8.64 GHz (right). Images are roughly  $45''$  on a side oriented with north up and east to the left. The beam shape for each frequency is shown in the bottom right corner. Flux density contour lines of  $-0.1$ ,  $0.1$ ,  $0.125$ ,  $0.15$ , and  $0.175 \text{ mJy beam}^{-1}$  are shown. The expected location of LHS 3003 is indicated by the large cross at center.

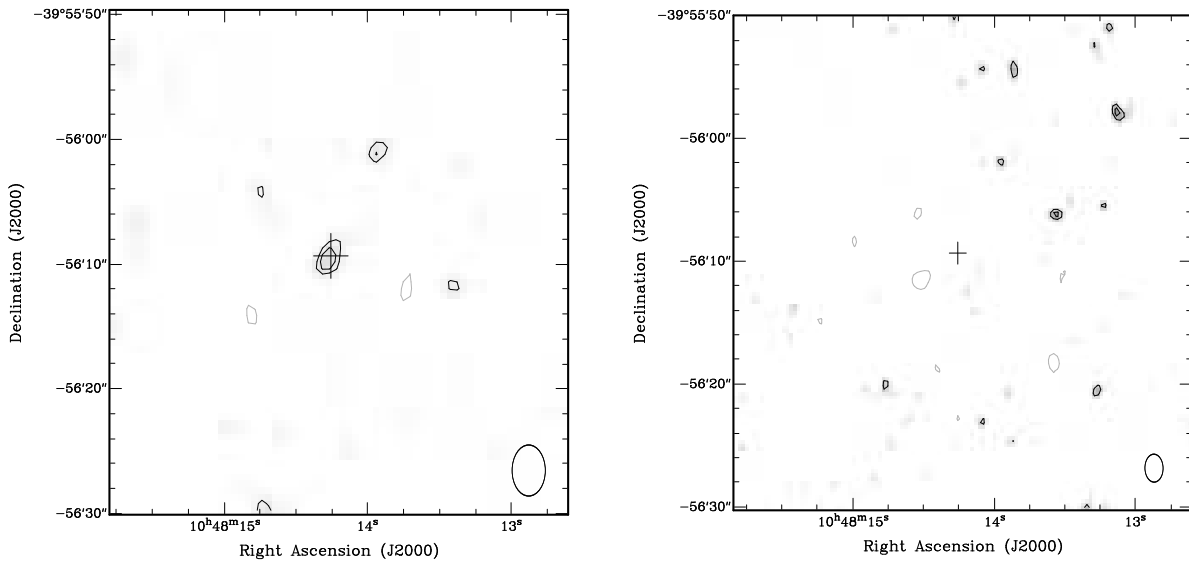


Fig. 2.— Same as Figure 1 for the M8 DENIS 1048–3956. Images are  $40''$  on a side. Visibility data during the observed flares (§ 4) have been excluded from these images.

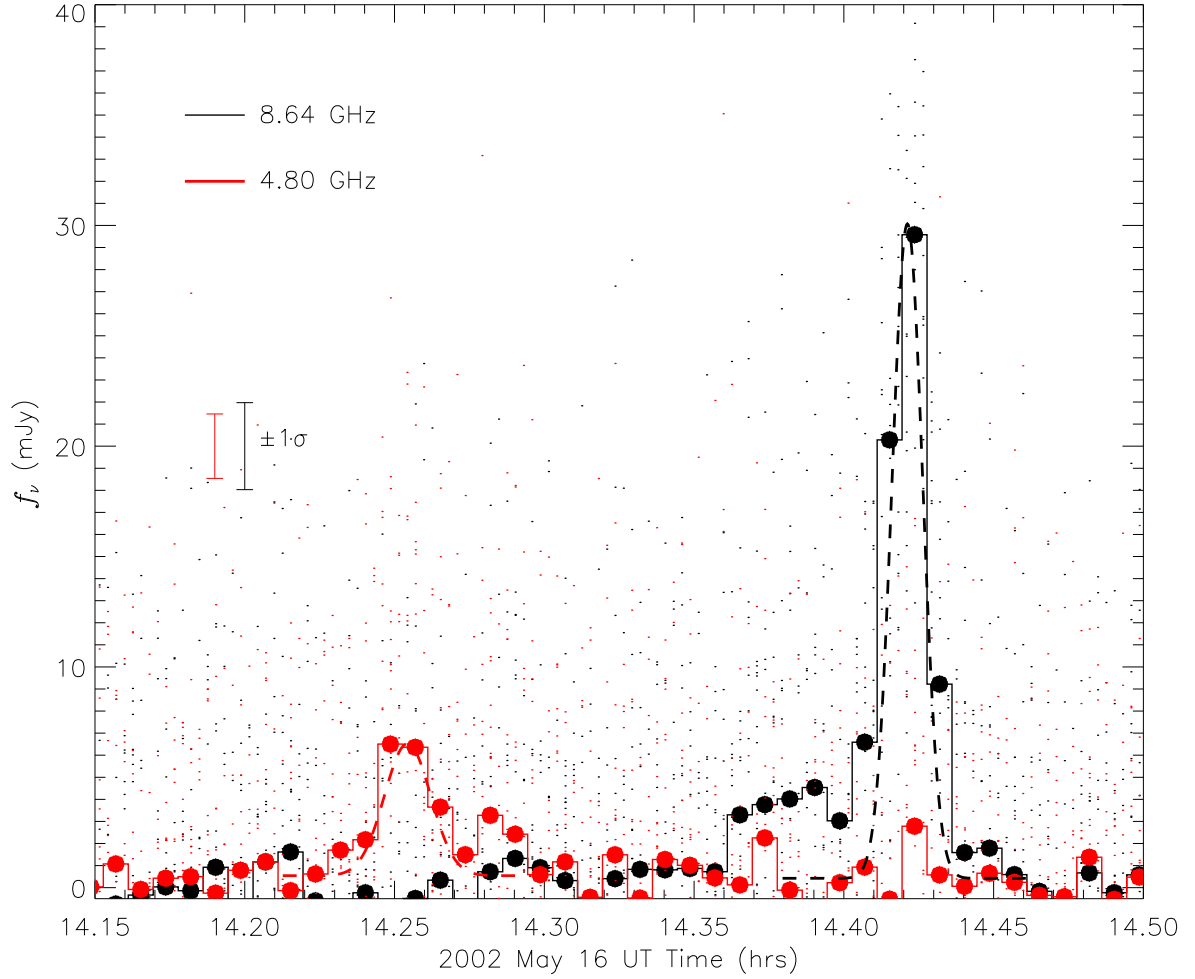


Fig. 3.— Time series data for the DENIS 1048-3956 flaring emission at 4.80 (red) and 8.64 GHz (black). The individual flux-calibrated visibility measurements are shown as small points; note the clear peak up in these data during the 8.64 GHz flare. Time-averaged visibilities (all baselines, central  $\Delta\nu = 72$  MHz, and 30 sec time resolution) are indicated by filled circles and histograms, and  $1\sigma$  error bars (based on the fluctuation of the binned data outside the flare periods) are indicated. The median background emission has been subtracted from these data. Gaussian fits to the un-binned visibility data during the flares at 14:15:15 (4.80 GHz) and 14:25:16 UT (8.64 GHz) are indicated by dashed lines.

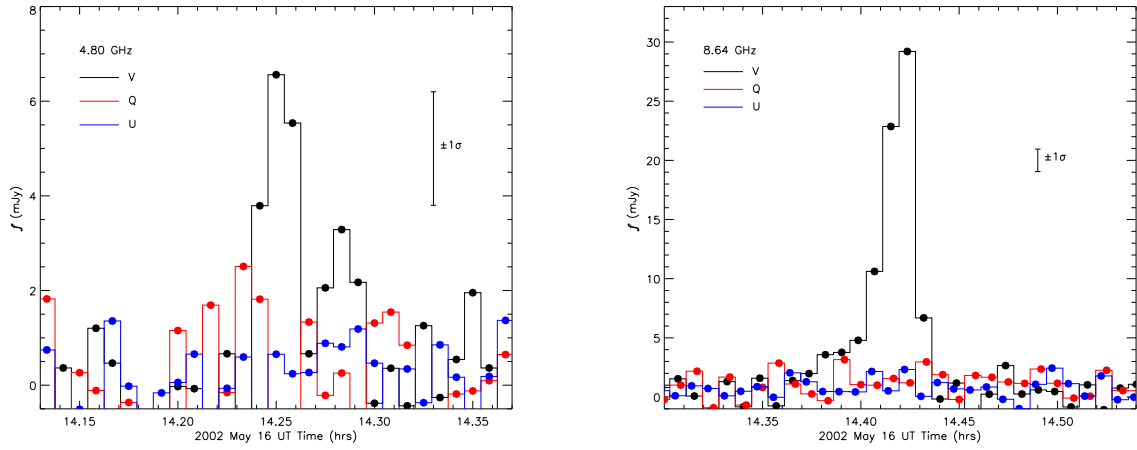


Fig. 4.— Time series data for the 4.80 (left) and 8.60 GHz (right) flares in Stokes V (black), Q (red), and U (blue) polarizations. Time-binned visibility data (30 s) for periods of 15 min about the flare peaks are indicated by filled circles and histograms. The median background/continuum emission has been subtracted from these data. Error bars ( $1\sigma$ , maximum for all three polarizations) were computed as in Figure 3.



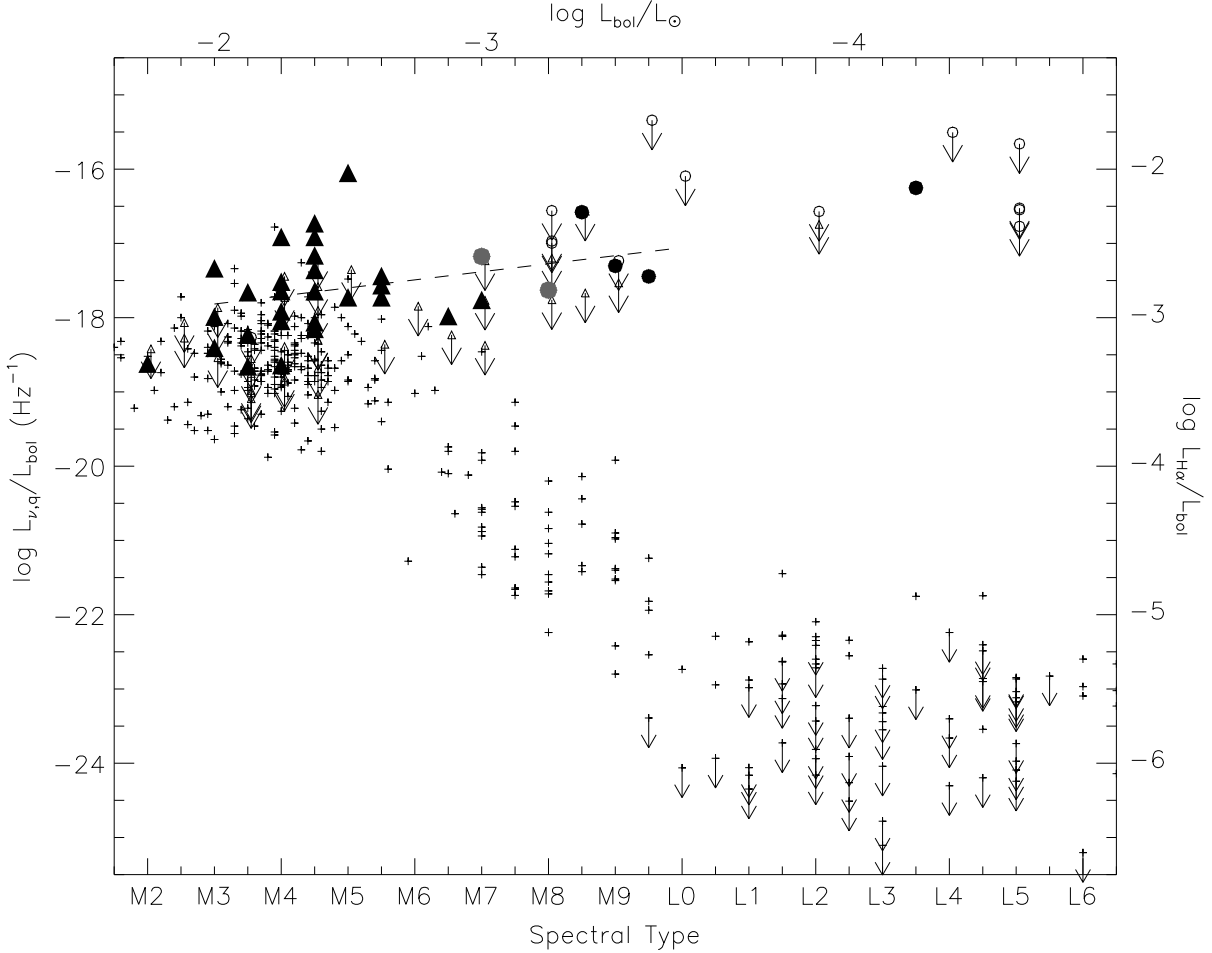


Fig. 5.— Ratio of quiescent radio (left axis) and  $H\alpha$  (right axis) to bolometric luminosity versus spectral type for late-type main sequence stars. M dwarf radio data from Linsky & Gary (1983); White, Jackson, & Kundu (1989); Güdel & Benz (1993); Krishnamurthi, Leto, & Linksy (1999); and Leto et al. (2000) are indicated by triangles, while ultracool (late-type M and L dwarf) data from B01, B02 (black), and this paper (grey) are indicated by circles. Open symbols with arrows indicate upper limits.  $H\alpha$  data from Hawley, Gizis, & Reid (1996); Gizis et al. (2000); and Burgasser et al. (2002a) are shown as crosses, and upper limits are indicated by arrows. Bolometric luminosities for all sources were derived from a seventh order polynomial fit to empirical values from the 8 pc sample (Reid & Hawley 2000) and Golimowski et al. (2004) for spectral types M0 to L7; standard deviation in the fit was 0.35 mag. A linear fit to  $\log L_{\nu,q}/L_{bol}$  for M3-M9 detected radio sources (Eqn. 5) is indicated by the dashed line.

Table 1. Late-type M and L Dwarf Targets.

Name	Coordinates <sup>a</sup>		SpT	$d$ (pc)	$T_{eff}$ (K)	$\log L_{bol}$ (erg s <sup>-1</sup> )	$\log L_X$ (erg s <sup>-1</sup> )	$v \sin i$ (km s <sup>-1</sup> )	H $\alpha$ Emission		References
	$\alpha_{J2000}$	$\delta_{J2000}$							Quies.	Flare	
(1)	(2)	(3)	(4)	(5)	(6)	(7)	(8)	(9)	(10)	(11)	(12)
LHS 102A	00 <sup>h</sup> 04 <sup>m</sup> 37 <sup>s</sup> .06	-40°44′07″.7	M3.5	9.55±0.10	3200	31.3	< 27.5	...	No	...	1,2,3,4
LHS 102B	00 <sup>h</sup> 04 <sup>m</sup> 35 <sup>s</sup> .07	-40°44′11″.5	L5	9.55±0.10	1900	29.6	< 27.5	32.5±2.5	Yes	...	2,4,5,6
SSSPM 0109-5100	01 <sup>h</sup> 09 <sup>m</sup> 01 <sup>s</sup> .53	-51°00′49″.7	L2	~ 10	2100	29.7	< 27.5	...	...	...	7,8,9
2MASS 0835-0819	08 <sup>h</sup> 35 <sup>m</sup> 42 <sup>s</sup> .56	-08°19′23″.7	L5	~ 8	1700	29.5	< 27.4	...	No	...	8,9,10
DENIS 1048-3956	10 <sup>h</sup> 48 <sup>m</sup> 14 <sup>s</sup> .26	-39°56′09″.3	M8	4.6±0.3	2500	30.2	< 26.3	25±2	Yes	Yes	9,11,12,13,14,15
2MASS 1139-3159 <sup>b</sup>	11 <sup>h</sup> 39 <sup>m</sup> 51 <sup>s</sup> .11	-31°59′21″.1	M8	~ 20	2500	30.2	< 28.2	...	Yes	...	8,9,12
LHS 3003	14 <sup>h</sup> 56 <sup>m</sup> 38 <sup>s</sup> .17	-28°09′50″.5	M7	6.56±0.15	2600	30.3	26.3	8.0±2.5	Yes	Yes	4,16,17,18,19,20
2MASS 1534-1418	15 <sup>h</sup> 34 <sup>m</sup> 57 <sup>s</sup> .04	-14°18′48″.6	M8	~ 11	2500	30.2	< 27.6	...	Yes	...	7,8,12

<sup>a</sup>J2000 coordinates from 2MASS (epoch 1998.5-1999.5) updated to the observation epoch (except for 2MASS 0835-0819 and 2MASS 1534-1418) using proper motion measurements from Tinney (1996); Delfosse et al. (2001); Gizis (2002); and Scholz & Meusinger (2002).

<sup>b</sup>TW Hyd candidate (Gizis 2002).

References. — (1) Luyten (1979a); (2) van Altena, Lee, & Hoffleit (1995); (3) Hawley, Gizis, & Reid (1996); (4) Leggett et al. (2002); (5) Goldman et al. (1999); (6) Basri et al. (2000); (7) Lodieu, Scholz, & McCaughrean (2002); (8) distance estimated using  $M_J$ /spectral type relation of Cruz et al. (2003); (9)  $T_{eff}$  and  $L$  estimated using spectral type relations of Golimowski et al. (2004); (10) Cruz et al. (2003); (11) Delfosse et al. (2001); (12) Gizis (2002); (13) Neuhäuser et al. (2002); (14) Fuhrmeister & Schmitt (2004); (15) Schmitt & Liefke (2004); (16) Bessell (1991); (17) Ianna (1995); (18) Schmitt, Fleming, & Giampapa (1995); (19) Mohanty & Basri (2003); (20) Ruiz et al. (1990)

Table 2. Log of Observations.

Object (1)	UT Time		$t_{track}$ (hr) (4)	Beam Size		Secondary Cal (7)
	Start (2)	Finish (3)		4.80 GHz (5)	8.64 GHz (6)	
LHS 102AB	2002 May 16 16:15	May 17 03:29	11.2	4''2×2''6	2''4×1''4	PKS B0008-421
SSSPM 0109-5100	2002 Dec 02 06:05	Dec 02 17:45	11.7	3''5×2''8	1''9×1''6	PKS B0047-579
2MASS 0835–0819	2002 Nov 29 13:16	Nov 30 23:02	9.8	25''7×2''2	14''3×1''2	PKS B0859-140
DENIS 1048–3956	2002 May 16 03:11	May 16 15:32	12.4	4''1×2''7	2''3×1''5	PKS B1104-445
2MASS 1139–3159	2002 Nov 30 14:47	Dec 01 01:39	10.9	4''9×2''6	2''7×1''5	PKS B1144-379
LHS 3003	2002 May 17 07:12	May 17 18:09	11.0	6''3×2''7	3''5×1''5	PKS B1514-241
2MASS 1534–1418	2002 Dec 01 19:24	Dec 02 05:28	10.1	13''0×2''5	7''2×1''4	PKS B1504-166

Table 3. Quiescent Emission.

Object (1)	$f_{4.80}$ (mJy) (2)	$f_{8.64}$ (mJy) (3)	$\alpha$ (4)	$\log L_{\nu,q}$ (erg s <sup>-1</sup> Hz <sup>-1</sup> ) (5)	$\log L_R/L_{bol}^a$ (6)	$T_B$ (K) <sup>b</sup>
LHS 102A	< 0.09	< 0.11	...	< 13.0	< -8.4	< 2×10 <sup>8</sup>
LHS 102B	< 0.09	< 0.11	...	< 13.0	< -6.7	< 2×10 <sup>8</sup>
SSSPM 0109–5100	< 0.11	< 0.11	...	< 13.1	< -6.7	< 7×10 <sup>7</sup>
2MASS 0835–0819	< 0.12	< 0.12	...	< 13.0	< -6.6	< 5×10 <sup>7</sup>
DENIS 1048–3956	0.14±0.04	< 0.11	< -0.4	12.6	-7.7	(3 – 6)×10 <sup>7</sup>
2MASS 1139–3159	< 0.12	< 0.10	...	< 13.7	< -6.5	< 3×10 <sup>8</sup>
LHS 3003	0.27±0.04	< 0.12	< -1.2	13.1	-7.3	(1 – 3)×10 <sup>8</sup>
2MASS 1534–1418	< 0.11	< 0.11	...	< 13.2	< -7.1	< 9×10 <sup>7</sup>

<sup>a</sup>Assuming a spectral energy distribution peaked at  $\nu_{pk} = 4.80$  GHz, with  $f_\nu \propto \nu^{2.5}$  below  $\nu_{pk}$  and  $f_\nu \propto \nu^{-1.5}$  above  $\nu_{pk}$  over the range  $\nu_{pk}/10 < \nu < 10\nu_{pk}$ ; see § 3.2.

<sup>b</sup>Assuming source dimension  $\mathcal{L} \sim (2-3) \times R_*$ , where  $R_* \approx 0.1R_\odot \approx 1 R_{Jup} = 7 \times 10^9$  cm for late-type M and L dwarfs. For the M3.5 V LHS 102A, we assume  $R_* \approx 0.2R_\odot$  based on interferometric radius measurements of similarly-typed M dwarfs by Lane, Boden, & Kulkarni (2001) and Segransan et al. (2003).

Table 4. Flaring Emission from DENIS 1048–3956 on 2002 May 16 (UT).

	4.80 GHz	8.64 GHz
$t_{pk}$ (UT) <sup>a</sup>	14:15:15±6 s	14:25:16±1 s
$f_{\nu,f}$ (mJy) <sup>a</sup>	6.0±0.8	29.6±1.0
$\Pi_Q$ (%) <sup>b</sup>	<18	<3
$\Pi_U$ (%) <sup>b</sup>	<20	<3
$\Pi_V$ (%) <sup>b</sup>	~100	~100
$T_B(\mathcal{L}/R_*)^{-2}$ (K) <sup>c</sup>	$(1.1\pm0.2)\times10^{10}$	$(1.7\pm0.2)\times10^{10}$
$\log L_{\nu,f}$ (erg s <sup>-1</sup> Hz <sup>-1</sup> )	14.2	14.9

<sup>a</sup>Emission peak time and flux density based on Gaussian fits to the unbinned times series data (Figure 3).

<sup>b</sup>Polarizations at flare peak; upper limits for  $\Pi_Q$  and  $\Pi_U$  are estimated from  $1\sigma$  uncertainties in the time series data.

<sup>c</sup>We assume  $R_* \approx R_{Jup} = 7\times10^9$  cm. For  $\mathcal{L} \lesssim 0.04R_*$ ,  $T_B \gtrsim 10^{13}$  K (see § 4.2).